AFRL-RV-PS-
TR-2012-0088

FORECASTING $F_{10.7}$ WITH SOLAR MAGNETIC FLUX TRANSPORT MODELING (POSTPRINT)

C. J. Henney, et al.

3 April 2012

Interim Report

AIR FORCE RESEARCH LABORATORY
Space Vehicles Directorate
3550 Aberdeen Ave SE
AIR FORCE MATERIEL COMMAND
KIRTLAND AIR FORCE BASE, NM 87117-5776

DTIC COPY

NOTICE AND SIGNATURE PAGE

Using Government drawings, specifications, or other data included in this document for any purpose other than Government procurement does not in any way obligate the U.S. Government. The fact that the Government formulated or supplied the drawings, specifications, or other data does not license the holder or any other person or corporation; or convey any rights or permission to manufacture, use, or sell any patented invention that may relate to them.

This report was cleared for public release by the 377 ABW Public Affairs Office and is available to the general public, including foreign nationals. Copies may be obtained from the Defense Technical Information Center (DTIC) (http://www.dtic.mil).

AFRL-RV-PS-TR-2012-0088 HAS BEEN REVIEWED AND IS APPROVED FOR PUBLICATION IN ACCORDANCE WITH ASSIGNED DISTRIBUTION STATEMENT.

//signed//	//signed//
Charles N. Arge	Joel B. Mozer
Project Manager, RVBXS	Chief, RVB

This report is published in the interest of scientific and technical information exchange, and its publication does not constitute the Government's approval or disapproval of its ideas or findings.

REPORT DOCUMENTATION PAGE

Form Approved
OMB No. 0704-0188

1. REPORT DATE *(DD-MM-YYYY)*	**2. REPORT TYPE**	**3. DATES COVERED** *(From - To)*
03-04-2012	Interim Report	01 Oct 2007 – 07 Nov 2011

4. TITLE AND SUBTITLE

Forecasting $F_{10.7}$ with Solar Magnetic Flux Transport Modeling (Postprint)

5a. CONTRACT NUMBER

5b. GRANT NUMBER

5c. PROGRAM ELEMENT NUMBER
61102F

6. AUTHOR(S)

C. J. Henney, W. A. Toussaint, S. M. White, and C. N. Arge

5d. PROJECT NUMBER
2301

5e. TASK NUMBER
PPM00005114

5f. WORK UNIT NUMBER
EF004379

7. PERFORMING ORGANIZATION NAME(S) AND ADDRESS(ES)

Air Force Research Laboratory
Space Vehicles Directorate
3550 Aberdeen Ave. SE
Kirtland AFB, NM 87117-5776

8. PERFORMING ORGANIZATION REPORT NUMBER

AFRL-RV-PS-TR-2012-0088

9. SPONSORING / MONITORING AGENCY NAME(S) AND ADDRESS(ES)

10. SPONSOR/MONITOR'S ACRONYM(S)

AFRL/RVBXS

11. SPONSOR/MONITOR'S REPORT NUMBER(S)

12. DISTRIBUTION / AVAILABILITY STATEMENT

Approved for public release; distribution is unlimited. (377ABW-2011-1565 dtd 7 Nov 2011)

13. SUPPLEMENTARY NOTES

SPACE WEATHER, VOL. 10, S02011, doi:10.1029/2011SW000748, 2012. Government Purpose Rights.

14. ABSTRACT

A new method is presented here to forecast the solar 10.7 cm (2.8 GHz) radio flux, abbreviated F10.7, utilizing advanced predictions of the global solar magnetic field generated by a flux transport model. Using indices derived from the absolute value of the solar magnetic field, we find good correlation between the observed photospheric magnetic activity and the observed F10.7 values. Comparing magnetogram data observed within 6 hours of the F10.7 measurements during the years 1993 through 2010, the Spearman correlation coefficient, rs, for an empirical model of F10.7 is found to be 0.98. In addition, we find little change in the empirical model coefficients and correlations between the first and second 9 year intervals of the 18 year period investigated. By evolving solar magnetic synoptic maps forward 1–7 days, this new method provides a realistic estimation of the Earth-side solar magnetic field distribution used to forecast F10.7. Spearman correlation values of approximately 0.97, 0.95, and 0.93 are found for 1 day, 3 day, and 7 day forecasts, respectively. The method presented here can be expanded to forecast other space weather parameters, e.g., total solar irradiance and extreme ultraviolet flux. In addition, near-term improvements to the F10.7 forecasting method, e.g., including far-side magnetic data with solar magnetic flux transport, are discussed.

15. SUBJECT TERMS

Photospheric field, flux transport model, solar wind, solar corona, data assimilation, solar wind forecasting

16. SECURITY CLASSIFICATION OF:			**17. LIMITATION OF ABSTRACT**	**18. NUMBER OF PAGES**	**19a. NAME OF RESPONSIBLE PERSON**
a. REPORT	**b. ABSTRACT**	**c. THIS PAGE**			Charles N. Arge
Unclassified	Unclassified	Unclassified	Unlimited	14	**19b. TELEPHONE NUMBER** *(include area code)*

This page intentionally left blank.

Forecasting $F_{10.7}$ with solar magnetic flux transport modeling

C. J. Henney,[1] W. A. Toussaint,[2] S. M. White,[1] and C. N. Arge[1]

Received 7 November 2011; revised 16 December 2011; accepted 19 December 2011; published 23 February 2012.

[1] A new method is presented here to forecast the solar 10.7 cm (2.8 GHz) radio flux, abbreviated $F_{10.7}$, utilizing advanced predictions of the global solar magnetic field generated by a flux transport model. Using indices derived from the absolute value of the solar magnetic field, we find good correlation between the observed photospheric magnetic activity and the observed $F_{10.7}$ values. Comparing magnetogram data observed within 6 hours of the $F_{10.7}$ measurements during the years 1993 through 2010, the Spearman correlation coefficient, r_s, for an empirical model of $F_{10.7}$ is found to be 0.98. In addition, we find little change in the empirical model coefficients and correlations between the first and second 9 year intervals of the 18 year period investigated. By evolving solar magnetic synoptic maps forward 1–7 days, this new method provides a realistic estimation of the Earth-side solar magnetic field distribution used to forecast $F_{10.7}$. Spearman correlation values of approximately 0.97, 0.95, and 0.93 are found for 1 day, 3 day, and 7 day forecasts, respectively. The method presented here can be expanded to forecast other space weather parameters, e.g., total solar irradiance and extreme ultraviolet flux. In addition, near-term improvements to the $F_{10.7}$ forecasting method, e.g., including far-side magnetic data with solar magnetic flux transport, are discussed.

Citation: Henney, C. J., W. A. Toussaint, S. M. White, and C. N. Arge (2012), Forecasting $F_{10.7}$ with solar magnetic flux transport modeling, *Space Weather*, *10*, S02011, doi:10.1029/2011SW000748.

1. Introduction

[2] Forecasting variations in the solar ultraviolet (UV) and extreme ultraviolet (EUV) flux is of great interest for space weather. To a large extent these fluxes control conditions in the ionosphere that play a major role in communications and navigation signals, e.g., of the ionospheric total electron content [e.g., *Richards et al.*, 1994; *Maruyama*, 2010]. Current UV and EUV forecast models commonly rely on auto-regressive and time series analysis of past solar measurements of, e.g., the sunspot number (SSN) and solar 10.7 cm (2.8 GHz) radio flux [e.g., *Chatterjee*, 2001; *Lean et al.*, 2009; *Huang et al.*, 2009], commonly abbreviated as $F_{10.7}$. Parameters such as SSN and $F_{10.7}$ are, in general, proxies for solar magnetic activity. For example, the SSN is commonly used to estimate $F_{10.7}$ for a given day. Though the SSN and $F_{10.7}$ relationship has correlated well in the past, *Svalgaard and Hudson* [2010] found this may no longer be the case for the current solar cycle. The correlation change with cycle may be linked to the observation that the magnetic field strengths of sunspot umbrae appear to be varying with time [*Penn and Livingston*, 2006; *Livingston and Penn*, 2009]. These findings highlight the need to look for better magnetic proxies for solar activity. We show here that the observed Earth-side solar magnetic field strength and distribution can be used to estimate $F_{10.7}$ surprisingly well.

[3] *Chapman and Boyden* [1986] demonstrated that photospheric magnetic field measurements can be used to model the solar total irradiance. By using disk-position weighted sums of weak ($10 \le |B| \le 100$ G) and strong ($|B| \ge 100$ G) magnetic fields (B) separately, Chapman and Boyden estimated the fluctuations of facular and sunspot regions. Using the same magnetic sum limits, without the disk-position weighting, *Ulrich* [1991] and *Parker et al.* [1998] revealed that such magnetic field indices could be used as a proxy for $F_{10.7}$. These sums of the absolute value of the solar magnetic field, measured from the 150 foot Solar Tower at the Mount Wilson Observatory (MWO), are referred to as the MPSI (Magnetic Plage Strength Index) and MWSI (Mount Wilson Spot Index). Extending the period of study by Chapman and Boyden to three solar cycles, *Jain and Hasan* [2004] also found that the MPSI and MWSI indices can be used to model the solar irradiance, while *Schmahl and Kundu* [1995, 1998] showed that radio measurements at a number of frequencies can be used to reproduce solar irradiance variations.

[1]Space Vehicles Directorate, Air Force Research Laboratory, Kirtland Air Force Base, New Mexico, USA.
[2]National Solar Observatory, Tucson, Arizona, USA.

[4] Expanding on work of *Ulrich* [1991] and *Parker et al.* [1998], we outline here a method for forecasting space weather-related solar indices using future estimates of the global flux distribution on the photosphere. Utilizing global photospheric magnetic maps of the solar surface, the future Earth-side magnetic activity is estimated from a flux transport model. We have selected $F_{10.7}$ for this study since it is an extremely accurate and reliable data product widely used as a proxy for solar magnetic activity. The analysis presented here could also be expanded to forecast EUV/UV and total solar irradiance [e.g., *Wenzler et al.*, 2006; *Krivova et al.*, 2009]. Solar sources of $F_{10.7}$ and magnetic flux transport models, along with the method used here to forecast $F_{10.7}$ and preliminary results, are discussed in this paper.

2. Solar Sources of $F_{10.7}$

[5] Solar 10.7 cm radio flux data have become one of the most widely used space weather indices for a number of reasons: $F_{10.7}$ arises at least in part from the same hot coronal plasma that produces the Sun's ionizing (UV, EUV and soft X-ray) flux [e.g., *Swarup et al.*, 1963; *Tapping and DeTracey*, 1990]; the measurement of $F_{10.7}$ is carried out using a very careful and highly repeatable calibration procedure [*Tapping and Charrois*, 1994]; and there is an important historical record of measurements back to 1947 that can be used, and is used here, to investigate long-term trends and correlations with other phenomena [*Covington and Medd*, 1949; *Covington*, 1969; *Tapping*, 1987].

[6] The emitting wavelength of 10.7 cm is at a critical point in the Sun's radio spectrum [e.g., *Schmahl and Kundu*, 1998; *White*, 1999]. At longer wavelengths, e.g., 20 cm, the variable component of the Sun's radio emission is dominated by thermal bremsstrahlung from the hot gas in the solar corona, which can be optically thick. At shorter wavelengths, e.g., 6 cm, the corona is always optically thin to thermal bremsstrahlung but regions of strong magnetic field in the corona can be optically thick due to gyroresonance emission [e.g., *White and Kundu*, 1997]. Where the ambient magnetic fields are strong enough for the electron gyrofrequency to be a low harmonic of the observing frequency, thermal gyroresonance becomes an important emission process. In weaker magnetic fields, thermal bremsstrahlung emission continues to be dominant. The wavelength of 10.7 cm lies in a regime where we expect thermal bremsstrahlung to be largely optically thin, and thus large gyroresonance sources over active regions can be seen through the coronal plasma as bright contributors to the radio flux. Plages outside active regions will contribute to $F_{10.7}$ via thermal bremsstrahlung, but, unlike active regions, plages generally do not have field strengths sufficiently strong in the corona to contribute gyroresonance emission to $F_{10.7}$. The relative contributions of bremsstrahlung and gyroresonance emission to $F_{10.7}$ remain a matter of contention: *Felli et al.* [1981] and *Schmahl and Kundu* [1998] argue that gyroresonance emission dominates the rotationally modulated component of $F_{10.7}$, while *Tapping and DeTracey* [1990] argue that thermal bremsstrahlung is the main contributor. Unfortunately, to date there have been no systematic high-spatial-resolution imaging measurements at the wavelength of 10.7 cm that can settle this question.

[7] Whichever emission dominates the variable component of $F_{10.7}$, we expect to observe at least a qualitative relationship between $F_{10.7}$ and magnetic activity. The emission measure of material at coronal temperatures over an active region that produces thermal bremsstrahlung at radio wavelengths and line emission at EUV wavelengths is believed to reflect the amount of coronal heating taking place on magnetic field lines: heat deposited in the corona is thought to propagate down field lines and heat chromospheric material at the foot points that in turn rises back into the corona [e.g., *Cargill and Klimchuk*, 2004, and references therein]. In turn, the rate of coronal heating is found to be linked to the amount of magnetic flux in the active region [e.g., *Golub et al.*, 1980]. Therefore the thermal bremsstrahlung emission at radio wavelengths depends strongly on magnetic features at the photosphere, and it is clear that gyroresonance emission, which requires strong magnetic fields in the solar corona, must depend on the magnetic field in active regions. While a few previous studies have addressed this relationship [*Ulrich*, 1991; *Parker et al.*, 1998], there has been extensive work comparing $F_{10.7}$ with the sunspot number [e.g., *Bouwer*, 1992; *Floyd et al.*, 2005; *Tapping et al.*, 2007; *Svalgaard and Hudson*, 2010; *Johnson*, 2011; *Tapping and Valdés*, 2011]. In this paper we determine a quantitative relationship between $F_{10.7}$ and solar magnetic fields and then take advantage of state-of-the-art modeling of future magnetic field distributions to predict $F_{10.7}$ several days ahead.

3. Global Solar Magnetic Flux Transport

[8] Solar magnetic flux transport models provide an estimate of the instantaneous global spatial distribution of the solar magnetic field. The goal of these models is to evolve the synoptic magnetic flux distribution and match observations by incorporating rotational, meridional, and supergranular diffusive surface transport processes to predict the magnetic field in locations where direct measurements are not available [e.g., *Devore et al.*, 1984; *Sheeley et al.*, 1987; *Worden and Harvey*, 2000; *Schrijver and De Rosa*, 2003, and references therein].

[9] One of the primary uses of such instantaneous global maps is as input to coronal and solar wind forecasting models, e.g., the Wang-Sheeley-Arge (WSA) model [*Arge and Pizzo*, 2000; *Arge et al.*, 2003, 2004]. Output from magnetic flux transport models aid to minimize non-physical monopole moments in the magnetic maps used to initialize the coronal and solar wind models. Such monopoles commonly occur in Carrington synoptic maps near the eastern limb as a result of merging newly observed data and during periods when the solar polar regions are not well observed from the Earth. The magnetic flux transport model used here is the Air Force Data Assimilation

Table 1. Empirical $F_{10.7}$ Model Coefficients (m_0, m_1, and m_2 From Equation (1)) and Correlation Coefficients From the Regression Fits for the 18 Year Period Studied (1993–2010), Along With the Corresponding Standard Deviations[a]

Period	Year Range	Coverage	<Forecast Time> (days)	m_0 (sfu)	m_1 (sfu/G)	m_2 (sfu/G)	r_s	r
Total	1993–2010	67.0%	0.13 ±0.05	66.08 ±0.09	8.508 ±0.11	16.56 ±0.18	0.98	0.97
			1.13 ±0.05	65.26 ±0.10	8.522 ±0.11	17.20 ±0.19	0.97	0.96
			3.13 ±0.05	65.00 ±0.10	10.76 ±0.10	15.90 ±0.22	0.96	0.95
			7.13 ±0.05	64.75 ±0.09	14.83 ±0.09	8.861 ±0.27	0.94	0.91
A	1993–2001	70.9%	0.15 ±0.05	65.41 ±0.14	8.153 ±0.14	16.81 ±0.22	0.98	0.97
			1.15 ±0.05	64.88 ±0.15	8.446 ±0.14	17.04 ±0.24	0.98	0.96
			3.15 ±0.05	64.80 ±0.15	10.90 ±0.13	15.46 ±0.27	0.96	0.94
			7.15 ±0.05	64.59 ±0.14	15.56 ±0.13	6.870 ±0.34	0.94	0.90
B	2002–2010	63.2%	0.12 ±0.05	66.31 ±0.12	9.058 ±0.18	16.92 ±0.31	0.97	0.98
			1.12 ±0.05	65.44 ±0.13	8.495 ±0.17	18.22 ±0.33	0.96	0.97
			3.12 ±0.05	65.14 ±0.13	10.50 ±0.16	17.02 ±0.37	0.94	0.96
			7.12 ±0.05	64.92 ±0.12	13.87 ±0.14	11.95 ±0.46	0.92	0.93

[a]The fit and correlation values are provided for the period split into two 9 year intervals: A (1993–2001) and B (2002–2010). The correlation values include the Spearman (r_s) and Pearson (r) coefficients. The percentage of days used within the period ranges (i.e., Total, A, and B) are shown in the coverage column. The table rows, within each of the three ranges, are for the mean forecast times. Note that the forecast times are slightly greater than the target time (i.e., 0, 1, 3, and 7 days).

Photospheric Flux Transport model, referred to as ADAPT [*Arge et al.*, 2010, 2011]. ADAPT utilizes a modified version of the Worden and Harvey (WH) flux transport model [*Worden and Harvey*, 2000].

[10] The modified WH flux transport model within ADAPT employs an ensemble of model realizations based on using a range of different model parameters constrained by the estimated errors of each parameter (e.g., meridional drift). The data assimilation method currently incorporated by ADAPT is the ensemble least squares method [*Arge et al.*, 2011]. The use of an ensemble of models is beneficial in two significant ways: first, the ensemble variance is utilized to estimate the model error when determining the relative weight given to new data and model calculations in the assimilation step; second, comparing the different ensemble members individually with observations (e.g., solar polar field strength and coronal hole boundaries) provides feedback to determine the magnitude and time dependent behavior of large scale magnetic flow patterns such as the meridional drift rates in each hemisphere. The $F_{10.7}$ forecast method outlined in the following section uses forecast synoptic maps generated by ADAPT to provide estimates of the Earth-side solar magnetic field distribution 1 to 7 days into the future.

4. Forecasting $F_{10.7}$ With Flux Transport

[11] The ADAPT global photospheric maps used for this study were created using line-of-sight magnetogram data from 1993 through 2010 from the Kitt Peak Vacuum Telescope (KPVT [*Jones et al.*, 1992]) and Vector Spectromagnetograph (VSM [*Henney et al.*, 2009]). A new map is generated by ADAPT each time an observed magnetogram is available. Typically, the KPVT and VSM full-disk magnetograms are available at a cadence of approximately one per day. If no magnetograms are available, a new ADAPT map is generated at a cadence of ~24 hours since the last map was created. The choice of KPVT and VSM data instead of, e.g., MDI (Michelson Doppler Interferometer) or MWO, is arbitrary and based on the development version of the ADAPT code. Other magnetograph input can be used with the method outlined below, with the caveat that the inferred photospheric field strengths between instruments can vary as much as a factor of 2 [*Jones et al.*, 1993; *Wenzler et al.*, 2004; *Thornton and Jones*, 2002; *Riley*, 2007]. *Jones et al.* [2004] found that the magnetic fields measured by the KPVT and VSM agree, generally, to within a few percent. The VSM magnetic sensitivity improved with new cameras in late 2009. In total, for the 18 years studied here, there are two magnetic strength discontinuities on the order of a few percent: September 2003 due to the switch from the KPVT to the VSM and January 2010 due to a camera upgrade in the VSM.

[12] For this study the ADAPT code was modified to create forecast maps 0 to 7 days in the future at 20 UT to synchronize with the $F_{10.7}$ measurements near local noon at Penticton, British Columbia, Canada (earlier measurements were made at Ottawa, Ontario [*Tapping*, 1987]). The 0 day maps are created to model how well nearly simultaneous photospheric magnetic observations correlate with measured values of $F_{10.7}$. The 0 day map is generated for 20 UT using the most recent available observed magnetogram (note that KPVT and VSM data are not acquired at the same time each day). Since the most recent data are always acquired before 20 UT, and ADAPT then advances the assimilated data to 20 UT, there is variability in the forecast time. The analysis here is restricted to days on which new data are available within a 6 hour window before 20 UT. With this acceptance window, the 0 day maps used for this study have been evolved forward 3.4 hours, on average, and thus will not perfectly represent photospheric magnetic conditions at 20 UT when $F_{10.7}$ is measured. The fourth column of Table 1 provides the

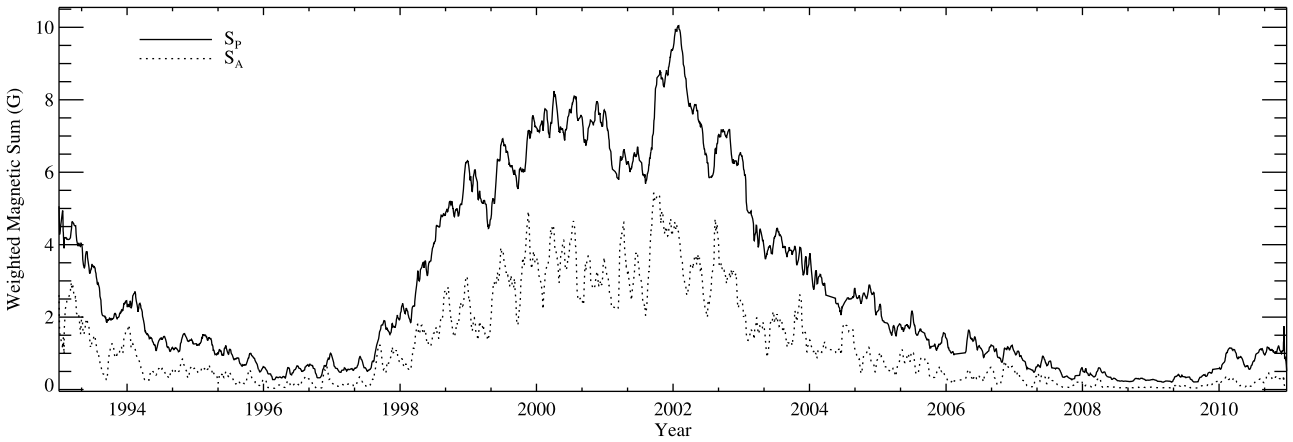

Figure 1. The weighted sums of the absolute magnetic fields, from Air Force Data Assimilation Photospheric Flux Transport model (ADAPT) Earth-side pixels, with values greater than 25 gauss and less than 150 gauss (i.e., a plage index, S_P, similar to the Magnetic Plage Strength Index (MPSI)) and greater than or equal to 150 gauss (i.e., an active region index, S_A, similar to the Mount Wilson Spot Index (MWSI)).

mean and standard deviation of the departure of the KPVT and VSM magnetogram observation time from 20 UT for the entire 18 years, and the first and last nine year periods.

[13] Comparable to the empirical model used by *Chapman and Boyden* [1986] and *Jain and Hasan* [2004] for modeling the total solar irradiance, we estimate the $F_{10.7}$ flux based on a fit to ADAPT-generated magnetic fields using ranges designed to separate the plage-dominated component from the sunspot-dominated component, analogous to the Magnetic Plage Strength Index and the Mount Wilson Spot Index. We tested over a dozen other magnetic field ranges and combinations, but found the fit and correlation improvements to be negligible. In addition, subdividing the magnetic fields into more than three ranges resulted in alternating negative coefficients. Since the fit improvements were negligible and do not justify the increased degrees of freedom, we chose to use two magnetic ranges.

[14] From ADAPT Earth-side map pixels, we compute the sums of the absolute magnetic field values greater than 25 gauss and less than 150 gauss (i.e., a plage index, S_P, similar to MPSI) and greater than or equal to 150 gauss (i.e., an active region index, S_A, similar to MWSI), to model $F_{10.7}$. Since the synoptic maps produced by ADAPT are in heliographic coordinates and hence essentially independent of the Sun-Earth distance, we model the values of $F_{10.7}$ adjusted to 1 AU in solar flux units (sfu), where 1 sfu is equivalent to 10^{-22} W m^{-2} Hz^{-1}. The empirical model used here is expressed as:

$$F_{\text{model}} = m_0 + m_1 S_P + m_2 S_A \quad (1)$$

where

$$S_P = \frac{1}{\sum \omega_\theta} \sum_{25G<|B_r|}^{|B_r|<150G} |B_r| \omega_\theta$$

$$S_A = \frac{1}{\sum \omega_\theta} \sum_{150G \le |B_r|} |B_r| \omega_\theta .$$

The variable ω_θ is a surface area weighting relative to latitude to convert the ADAPT map (i.e., 180 latitude by 360 longitude pixels) values to equal area. The normalization sum, identical for both S_P and S_A, is over all of the 180^2 Earth-side pixels. The magnetic field is represented by B_r to emphasize that the fields are radial for the ADAPT heliographic frame maps, where the radial field is derived from the magnetograms assuming that the observed field values are the line-of-sight component of a radial field. We derived the best-fit coefficients for equation (1) separately for 0, 1, 3, and 7 day ADAPT forecasts generated from all available daily magnetograms, for the total 18 years and the first and last nine years, which are shown in Table 1.

[15] Note that the default 180^2 pixel area used encompasses pixels that would not normally be observed in a sky-frame full-disk image. Earlier versions of the forecast method estimated the actual observed area as viewed from Earth, taking into account the solar tilt angle relative to Earth's orbit, along with the viewing angle relative to the Earth-Sun distance. The differences in spatial weighting, however, resulted in negligible improvements in the final fits and correlations. With the low resolution of the ADAPT maps, and the lack of the strong fields in polar regions that are normally associated with $F_{10.7}$, we chose to use 180^2 area from the maps for this preliminary study. The sum values for both S_P and S_A are shown in Figure 1. In the figure, note that the S_A values are rather flat during

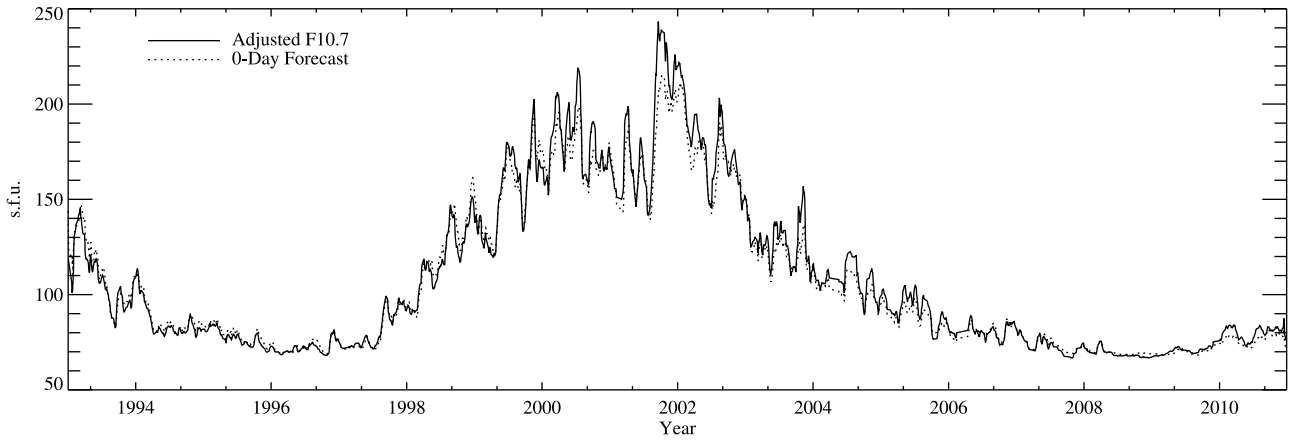

Figure 2. Adjusted observed $F_{10.7}$ (solid line) and the empirical model (dotted line), smoothed with a 21 day running mean, for the 18 year period studied. Note that periods with straight lines are generally associated with Vector Spectromagnetograph (VSM) instrument downtime (e.g., April–June 2004, February–April 2006, and December 2009).

the exceptional low activity period during late 2008 and early 2009 compared to the previous minimum. The higher variability of the stronger field regions is most likely a result of the smaller spatial scale and shorter lifetime of strong fields, i.e., sunspot regions.

5. Results and Discussion

[16] The 0 day ADAPT-derived $F_{10.7}$ values and the observed (adjusted to 1 AU) $F_{10.7}$ values for the full 18 year period (1993 through 2010) are compared in Figure 2. The figure highlights the good agreement between the two time series, but also reveals that the model values are generally too large during minimum solar magnetic activity and too weak during solar maximum activity. A more detailed comparison between the observed (forecast valid-time) values and the 1 day and 3 day forecasts is exhibited in Figure 3. With new activity rotating onto the Earth-side for the first time, the ADAPT maps are expected to exhibit a phase lag since they do not incorporate solar far-side data, such as helioseismic inferences of the emergence of new regions. Without information about activity on the far side of the Sun, the first knowledge of new magnetic activity is its appearance on the east limb provided by solar rotation, where observational errors are typically much higher than the model errors. The observational errors arise primarily from foreshortening and the canopy effect, along with the highly variable horizontal magnetic signal that increases toward the limb [*Harvey et al.*, 2007]. Since the model error is small by comparison, the observed data can take a few days to be fully assimilated.

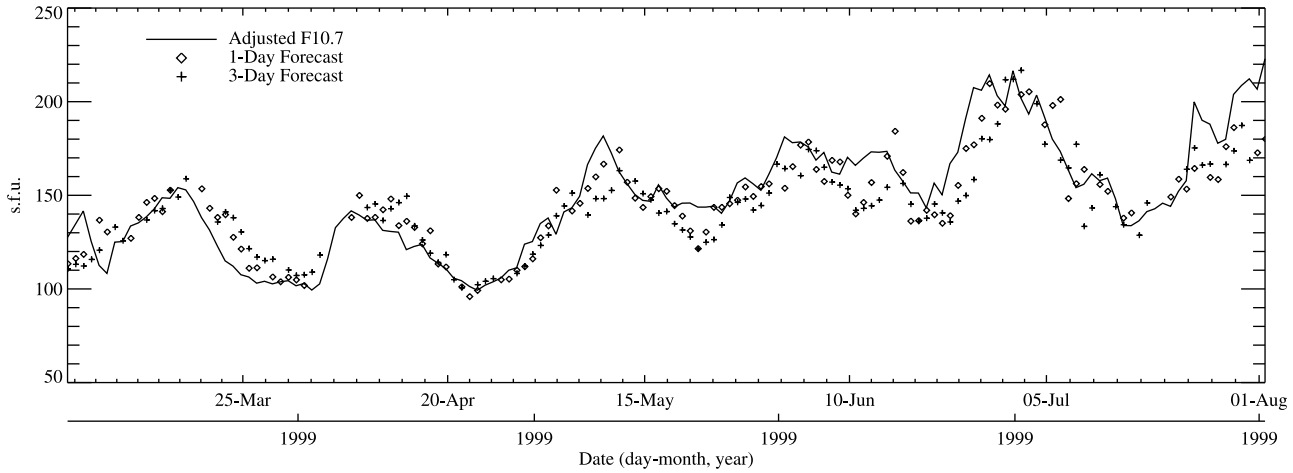

Figure 3. An example period of increasing solar magnetic activity showing daily values of the adjusted observed $F_{10.7}$ (solid line), modeled 1 day (diamond), and 3 day (plus sign) forecast estimations.

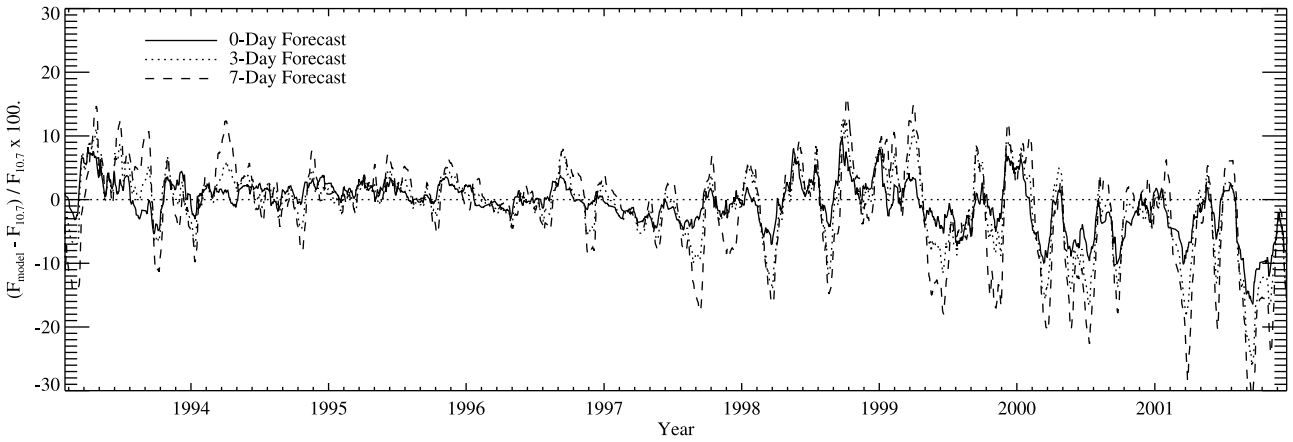

Figure 4. Interval A (1993–2001), the percent difference between the 0 day (solid), 3 day (dotted), and 7 day (dashed) ADAPT forecasts, and the adjusted observed $F_{10.7}$ values. Smoothed with a 21 day running mean, the differences highlight how the forecasts generally underestimate $F_{10.7}$ during high activity (1999–2001).

[17] Figures 4 and 5 display the percent difference between the 0, 3, and 7 day model values and observations for the 18 years split into two intervals: 1993 through 2001 (interval A) and 2002 through 2010 (interval B). These figures highlight when the empirical model is best (during low activity variability) and worst (during high variability) with differences between the model and observations ranging from a few percent to 25% for the 3 day values. Besides the lack of far-side magnetic activity information, this may reflect the fact that the strong field regions are not well represented with the nominal spatial resolution of ADAPT maps, i.e., 360 by 180 (longitude by latitude) pixels. It may also represent a change in the relative contributions to $F_{10.7}$ by gyroresonance and thermal bremsstrahlung emission at high activity levels. Comparing Figures 1 and 2, note that nearly all the variability of the $F_{10.7}$ signal correlates well with the magnetic active region sum, S_A. Attempts to fit the $F_{10.7}$ signal with only S_A resulted in a good fit in general, however, the local minima were underestimated. That is, once prominent activity rotated off the Earth-side, the $F_{10.7}$ background level is not well matched with S_A alone, and S_P, representing weaker fields, is needed to encompass the observed variability.

[18] For the 3 day ADAPT forecast maps, nearly 80% of the Earth-side pixels have been evolved for 72 hours or longer and ~20% of the pixels have been evolved for approximately 13 days or greater since the last Earth-side magnetogram observation. If the flux transport model of ADAPT were "perfect," the 0 day $F_{10.7}$ empirical model coefficients would be expected to be equally valid for the 1 through 7 day forecast maps, however, the mid-range magnetic fields tend to decrease faster in the model

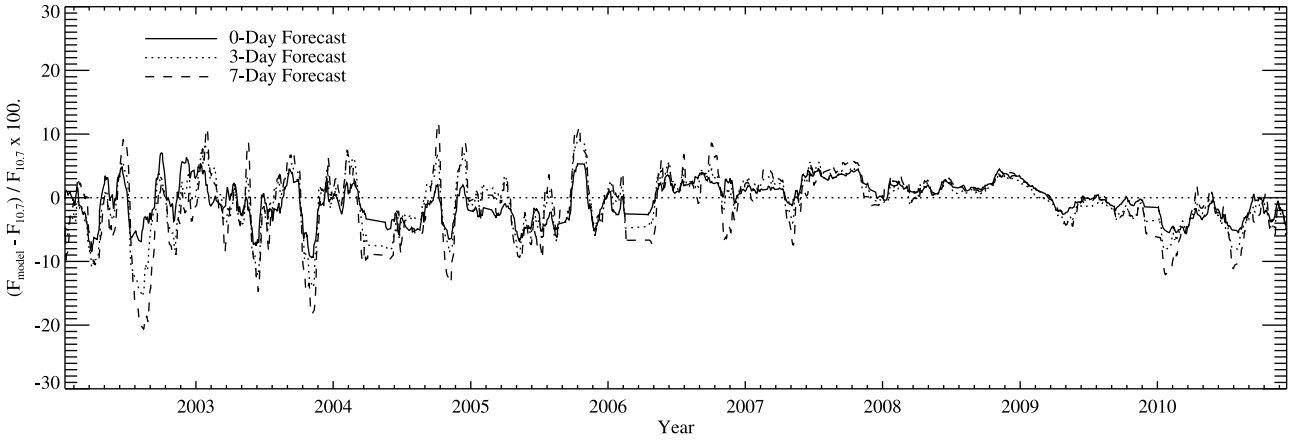

Figure 5. Interval B (2002–2010), the percent difference between the 0 day (solid), 3 day (dotted), and 7 day (dashed) ADAPT forecasts, and the adjusted observed $F_{10.7}$ values. Smoothed with a 21 day running mean, the differences highlight how the forecasts generally underestimate $F_{10.7}$ during high activity (2002–2006).

calculations than in the observations. The change is reflected in the increase of the m_1 coefficient value from 0 day to 7 day forecasts for all period fits in Table 1. The general amplitude drop could be the result of new background (i.e., weak field) and active region emergence not accounted for or too much flux diffusion comprised within the modeled supergranular flow. Since the Worden and Harvey flux transport within the ADAPT model applies far less diffusion to the strong magnetic fields [see *Worden and Harvey*, 2000], the drop is expected to be primarily from the weak fields. By fitting the different forecast maps (e.g., 0 day and 7 day) separately, this lack of mid-range flux can clearly be accounted for by the quality of the correlations. The mid-range flux drop was not detected until this work, and highlights how forecasting global indices can provide unique feedback to flux transport models. The lack of additional emergence or excessive diffusion will be addressed by an ongoing study to validate the flux transport model on varying timescales, from 12 hours to 6 days with Earth-side activity and 13 to 15 days for returning activity.

[19] The difference between the fit coefficients for the two 9 year intervals and the total period is found to be small, as depicted in Table 1, and well within the uncertainty in the scaling between the KPVT and VSM magnetograms for this period. The effect of this difference is minimal as demonstrated by the fact that using the interval A coefficients to determine the interval B radio flux values results in a correlation decrease of less than one half of a percent. The Spearman correlation values, using interval A coefficients, match those found fitting interval B independently with 0.97, 0.96, 0.94, and 0.94 for the 0, 1, 3, and 7 day forecasts respectively. The ability to interchange coefficients supports the argument that the relationship between $F_{10.7}$ and the $S_{A,P}$ parameters does not exhibit cycle-to-cycle variations. In addition, the stability of the coefficients reinforces the idea that magnetic parameters similar to $S_{A,P}$ are to be preferred as solar activity proxies over parameters such as the sunspot number, which has recently been shown to have a cycle-to-cycle dependence [*Penn and Livingston*, 2006; *Livingston and Penn*, 2009]. When the 18 year period is subdivided into spans less than 9 years (e.g., 5 years), the fits are dominated by either high activity or inactivity leading to poor forecasting once the activity trend changes. In addition, as stated earlier, we chose to use two magnetic ranges for the model even though the fits could be improved (albeit very slightly) by splitting the magnetic range into three or more bins. We found that the coefficients from fits using more than two ranges differed greatly between the two intervals, most likely because the additional bins simply allow for more degrees of freedom for the fit.

6. Near-Future Goals and Improvements

[20] A better understanding of the sources of the solar 10.7 cm radio flux signal is critical to improving the current empirical model development and evolving to a model atmospheric solution. For example, higher field thresholds for the active region index in equation (1) were tested with negligible improvement and greater uncertainty in the fitted coefficients. With higher spatial resolution maps, however, we might expect improved fits using a higher field threshold corresponding to the third harmonic of the gyrofrequency [e.g., *White and Kundu*, 1997], i.e., 333 gauss in the corona, once the relative contribution of bremsstrahlung and gyroresonance emission is better understood. With full-disk $F_{10.7}$ observations from the EVLA (Expanded Very Large Array) proposed in the near-future, we expect to achieve a more detailed understanding of the $F_{10.7}$ source locations in relation to the photospheric magnetic field. The planned comparison work between EVLA and magnetogram image data is anticipated to aid in the determination of the minimum spatial resolution for the global magnetic maps needed to improve future $F_{10.7}$ forecast models. In addition, the observational study is expected to provide feedback on the limitations of a simple empirical model outlined in the previous section. The benefit of using magnetic flux transport with global solar magnetic maps is that we can move away from an empirical model toward a physics-based model for forecasting $F_{10.7}$ [e.g., *Lionello et al.*, 2009]. Ultimately, daily spatially resolved $F_{10.7}$ observations [see *Saint-Hilaire et al.*, 2012] would permit long-term feedback and refinement of flux transport models like ADAPT.

[21] While the current version of the ADAPT-driven empirical model proves to be practical for estimating the $F_{10.7}$ value for forecast timescales of 1 to 3 days, including solar far-side magnetic activity estimates will be key to modeling more accurate forecast values and extending forecasts to 7 days. The far-side estimates are possible with the helioseismic acoustic holography technique [e.g., *Lindsey and Braun*, 1990, 1997] that can detect large magnetic regions on the solar far-side. The helioseismic far-side detection technique has recently been parametrized in terms of photospheric magnetic field strength [*González Hernández et al.*, 2007], allowing for a quantitative estimation of the solar magnetic activity on the solar far-side while updating the Earth-side of global synoptic maps. The practical application of the far-side data has recently been demonstrated to agree well with the observed $F_{10.7}$ signal [*González Hernández et al.*, 2011]. The inclusion of far-side data with ADAPT is part of a newly funded 3 year study. The ADAPT model is ideal for representing the nominal distribution and morphology of the far-side active region polarity (e.g., Hale's rule) and orientation (e.g., Joy's rule) within the ensemble realizations. Though the flux polarity and distribution will have large uncertainty, a good estimate of the inferred magnetic flux location and magnitude is all that is required to improve the $F_{10.7}$ forecast.

7. Summary

[22] The solar 10.7 cm radio flux forecast method presented here is shown to agree well with observation,

resulting in Spearman correlation values of 0.97, 0.95 and 0.93 for 1, 3, and 7 day forecasts, respectively. The empirical model developed here is based on the estimation of the future global solar photospheric magnetic field using the flux transport of the ADAPT model. By evolving solar magnetic synoptic maps forward 1 to 7 days, this method provides a realistic estimation of the Earth-side solar magnetic field distribution and a key preliminary step toward more physics-driven forecasting of space weather parameters. As the ADAPT model is updated in the near-future with solar far-side input, along with flux transport model parameter improvements from forthcoming validation work, we expect improved agreement between forecasts and $F_{10.7}$ observations. Ultimately, the disagreement between forecast values and observations may provide useful feedback for the selection of ADAPT model parameters within the model ensemble. In addition, with higher spatial resolution we fully expect that flux transport models similar to ADAPT could be used to forecast the total solar irradiance and the sunspot number, in addition to solar wind, $F_{10.7}$, ultraviolet and extreme ultraviolet flux.

[23] **Acknowledgments.** We are grateful to Luca Bertello and John Harvey for helpful discussions regarding the scaling of VSM magnetogram data. In addition, we gratefully acknowledge the two referees for helpful comments and suggestions. The work presented here was partially supported by the AFRL's (Air Force Research Laboratory) Space Weather Forecasting Laboratory (SWFL). The ADAPT software used in this work was developed with support by a grant from the AFOSR (Air Force Office of Scientific Research). The 10.7 cm solar radio flux data service is operated by the National Research Council of Canada and Natural Resources Canada, with the support of the Canadian Space Agency. The National Solar Observatory (NSO) data used for this work are produced cooperatively by National Science Foundation (NSF) and the NSO. The NSO is operated by the Association of Universities for Research in Astronomy (AURA), Inc., under cooperative agreement with the NSF.

References

Arge, C. N., and V. J. Pizzo (2000), Improvement in the prediction of solar wind conditions using near-real time solar magnetic field updates, *J. Geophys. Res.*, *105*, 10,465–10,480, doi:10.1029/1999JA900262.

Arge, C. N., D. Odstrcil, V. J. Pizzo, and L. R. Mayer (2003), Improved method for specifying solar wind speed near the Sun, in *Solar Wind Ten*, edited by M. Velli, F. Malara, and R. Bruno, *AIP Conf. Proc.*, *679*, 190–193, doi:10.1063/1.1618574.

Arge, C. N., J. G. Luhmann, D. Odstrcil, C. J. Schrijver, and Y. Li (2004), Stream structure and coronal sources of the solar wind during the May 12th, 1997 CME, *J. Atmos. Sol. Terr. Phys.*, *66*, 1295–1309, doi:10.1016/j.jastp.2004.03.018.

Arge, C. N., C. J. Henney, J. Koller, C. R. Compeau, S. Young, D. MacKenzie, A. Fay, and J. W. Harvey (2010), Air Force Data Assimilative Photospheric Flux Transport (ADAPT) model, in *Solar Wind Twelve*, *AIP Conf. Proc.*, *1216*, 343–346, doi:10.1063/1.3395870.

Arge, C. N., C. J. Henney, J. Koller, W. A. Toussaint, J. W. Harvey, and S. Young (2011), Improving data drivers for coronal and solar wind models, in *5th International Conference of Numerical Modeling of Space Plasma Flows (ASTRONUM 2010)*, *ASP Conf. Ser.*, vol. 444, edited by N. V. Pogorelov, E. Audit, and G. P. Zank, p. 99, Astron. Soc. of the Pac., San Francisco, Calif.

Bouwer, S. D. (1992), Periodicities of solar irradiance and solar activity indices: II, *Sol. Phys.*, *142*, 365–389, doi:10.1007/BF00151460.

Cargill, P. J., and J. A. Klimchuk (2004), Nanoflare heating of the corona revisited, *Astrohys. J.*, *605*, 911–920, doi:10.1086/382526.

Chapman, G. A., and J. E. Boyden (1986), Solar irradiance variations derived from magnetograms, *Astrophys. J.*, *302*, L71–L73, doi:10.1086/184640.

Chatterjee, T. N. (2001), On the application of information theory to the optimum state-space reconstruction of the short-term solar radio flux (10.7 cm), and its prediction via a neural network, *Mon. Not. R. Astron. Soc.*, *323*, 101–108, doi:10.1046/j.1365-8711.2001.04110.x.

Covington, A. E. (1969), Solar radio emission at 10.7 cm, 1947–1968, *J. R. Astron. Soc. Can.*, *63*, 125.

Covington, A. E., and W. J. Medd (1949), Simultaneous observations of solar radio noise on 1.5 meters and 10.7 centimeters, *J. R. Astron. Soc. Can.*, *43*, 106.

Devore, C. R., J. P. Boris, and N. R. Sheeley Jr. (1984), The concentration of the large-scale solar magnetic field by a meridional surface flow, *Sol. Phys.*, *92*, 1–14, doi:10.1007/BF00157230.

Felli, M., K. R. Lang, and R. F. Willson (1981), VLA observations of solar active regions: II. Solar bursts, *Astrophys. J.*, *247*, 338, doi:10.1086/159042.

Floyd, L., J. Newmark, J. Cook, L. Herring, and D. McMullin (2005), Solar EUV and UV spectral irradiances and solar indices, *J. Atmos. Sol. Terr. Phys.*, *67*, 3–15, doi:10.1016/j.jastp.2004.07.013.

Golub, L., C. Maxson, R. Rosner, G. S. Vaiana, and S. Serio (1980), Magnetic fields and coronal heating, *Astrophys. J.*, *238*, 343–348, doi:10.1086/157990.

González Hernández, I., F. Hill, and C. Lindsey (2007), Calibration of seismic signatures of active regions on the far side of the Sun, *Astrophys. J.*, *669*, 1382–1389, doi:10.1086/521592.

González Hernández, I., K. Jain, W. K. Tobiska, and F. Hill (2011), The far-side solar magnetic index, *J. Phys. Conf. Ser.*, *271*, 012028, doi:10.1088/1742-6596/271/1/012028.

Harvey, J. W., et al. (2007), Seething horizontal magnetic fields in the quiet solar photosphere, *Astrophys. J.*, *659*, L177–L180, doi:10.1086/518036.

Henney, C. J., C. U. Keller, J. W. Harvey, M. K. Georgoulis, N. L. Hadder, A. A. Norton, N.-E. Raouafi, and R. M. Toussaint (2009), SOLIS vector spectromagnetograph: Status and science, in *Solar Polarization 5: In Honor of Jan Stenflo*, *ASP Conf. Ser.*, vol. 405, edited by S. V. Berdyugina, K. N. Nagendra, and R. Ramelli, p. 47, Astron. Soc. of the Pac., San Francisco, Calif.

Huang, C., D.-D. Liu, and J.-S. Wang (2009), Forecast daily indices of solar activity, F10.7, using support vector regression method, *Res. Astron. Astrophys.*, *9*, 694–702, doi:10.1088/1674-4527/9/6/008.

Jain, K., and S. S. Hasan (2004), Modulation in the solar irradiance due to surface magnetism during cycles 21, 22 and 23, *Astron. Astrophys.*, *425*, 301–307, doi:10.1051/0004-6361:20047102.

Johnson, R. W. (2011), Power law relating 10.7 cm flux to sunspot number, *Astrophys. Space Sci.*, *332*, 73–79, doi:10.1007/s10509-010-0500-1.

Jones, H. P., T. L. Duvall Jr., J. W. Harvey, C. T. Mahaffey, J. D. Schwitters, and J. E. Simmons (1992), The NASA/NSO spectromagnetograph, *Sol. Phys.*, *139*, 211–232, doi:10.1007/BF00159149.

Jones, H., et al. (1993), A magnetograph comparison workshop, *Bull. Am. Astron. Soc.*, *25*, 1216.

Jones, H. P., J. W. Harvey, C. J. Henney, C. U. Keller, and O. M. Malanushenko (2004), Measurement scale of the SOLIS vector spectromagnetograph, *Bull. Am. Astron. Soc.*, *36*, 709.

Krivova, N. A., S. K. Solanki, T. Wenzler, and B. Podlipnik (2009), Reconstruction of solar UV irradiance since 1974, *J. Geophys. Res.*, *114*, D00I04, doi:10.1029/2009JD012375.

Lean, J. L., J. M. Picone, and J. T. Emmert (2009), Quantitative forecasting of near-term solar activity and upper atmospheric density, *J. Geophys. Res.*, *114*, A07301, doi:10.1029/2009JA014285.

Lindsey, C., and D. C. Braun (1990), Helioseismic imaging of sunspots at their antipodes, *Sol. Phys.*, *126*, 101–115, doi:10.1007/BF00158301.

Lindsey, C., and D. C. Braun (1997), Helioseismic holography, *Astrophys. J.*, *485*, 895, doi:10.1086/304445.

Lionello, R., J. A. Linker, and Z. Mikić (2009), Multispectral emission of the Sun during the first whole Sun month: Magnetohydrodynamic simulations, *Astrophys. J.*, *690*, 902–912, doi:10.1088/0004-637X/690/1/902.

Livingston, W., and M. Penn (2009), Are sunspots different during this solar minimum?, *Eos Trans. AGU*, *90*(30), 257–258, doi:10.1029/2009EO300001.

Maruyama, T. (2010), Solar proxies pertaining to empirical ionospheric total electron content models, *J. Geophys. Res.*, *115*, A04306, doi:10.1029/2009JA014890.

Parker, D. G., R. K. Ulrich, and J. M. Pap (1998), Modeling solar UV variations using Mount Wilson Observatory indices, *Sol. Phys.*, *177*, 229–241.

Penn, M. J., and W. Livingston (2006), Temporal changes in sunspot umbral magnetic fields and temperatures, *Astrophys. J.*, *649*, L45–L48, doi:10.1086/508345.

Richards, P. G., J. A. Fennelly, and D. G. Torr (1994), EUVAC: A solar EUV flux model for aeronomic calculations, *J. Geophys. Res.*, *99*, 8981–8992, doi:10.1029/94JA00518.

Riley, P. (2007), An alternative interpretation of the relationship between the inferred open solar flux and the interplanetary magnetic field, *Astrophys. J.*, *667*, L97–L100, doi:10.1086/522001.

Saint-Hilaire, P., G. J. Hurford, G. Keating, G. C. Bower, and C. Gutierrez-Kraybill (2012), Allen Telescope Array multi-frequency observations of the Sun, *Sol. Phys.*, in press.

Schmahl, E. J., and M. R. Kundu (1995), Microwave proxies for sunspot blocking and total irradiance, *J. Geophys. Res.*, *100*, 19,851–19,864, doi:10.1029/95JA00677.

Schmahl, E. J., and M. R. Kundu (1998), Synoptic radio observations, in *Synoptic Solar Physics*, *ASP Conf. Ser.*, vol. 140, edited by K. S. Balasubramaniam, J. W. Harvey, and D. Rabin, p. 387, Astron. Soc. of the Pac., San Francisco, Calif.

Schrijver, C. J., and M. L. De Rosa (2003), Photospheric and heliospheric magnetic fields, *Sol. Phys.*, *212*, 165–200, doi:10.1023/A:1022908504100.

Sheeley, N. R., Jr., A. G. Nash, and Y.-M. Wang (1987), The origin of rigidly rotating magnetic field patterns on the Sun, *Astrophys. J.*, *319*, 481–502, doi:10.1086/165472.

Svalgaard, L., and H. S. Hudson (2010), The solar microwave flux and the sunspot number, in *SOHO-23: Understanding a Peculiar Solar Minimum*, *ASP Conf. Ser.*, vol. 428, edited by S. R. Cranmer, J. T. Hoeksema, and J. L. Kohl, p. 325, Astron. Soc. of the Pac., San Francisco, Calif.

Swarup, G., T. Kakinuma, A. E. Covington, G. A. Harvey, R. F. Mullaly, and J. Rome (1963), High-resolution studies of ten solar active regions at wavelengths of 3–21 cm, *Astrophys. J.*, *137*, 1251, doi:10.1086/147601.

Tapping, K. F. (1987), Recent solar radio astronomy at centimeter wavelengths: The temporal variability of the 10.7-cm flux, *J. Geophys. Res.*, *92*, 829–838, doi:10.1029/JD092iD01p00829.

Tapping, K. F., and D. P. Charrois (1994), Limits to the accuracy of the 10.7 cm flux, *Sol. Phys.*, *150*, 305–315, doi:10.1007/BF00712892.

Tapping, K. F., and B. DeTracey (1990), The origin of the 10.7 cm flux, *Sol. Phys.*, *127*, 321–332, doi:10.1007/BF00152171.

Tapping, K. F., and J. J. Valdés (2011), Did the Sun change its behaviour during the decline of cycle 23 and into cycle 24?, *Sol. Phys.*, *272*, 337–350, doi:10.1007/s11207-011-9827-1.

Tapping, K. F., D. Boteler, P. Charbonneau, A. Crouch, A. Manson, and H. Paquette (2007), Solar magnetic activity and total irradiance since the Maunder Minimum, *Sol. Phys.*, *246*, 309–326, doi:10.1007/s11207-007-9047-x.

Thornton, C. E., and H. P. Jones (2002), Comparison of three solar magnetographs, *Bull. Am. Astron. Soc.*, *34*, 1243.

Ulrich, R. K. (1991), A co-ordinated and synergistic analysis strategy for future ground-based and space helioseismology, *Adv. Space Res.*, *11*, 217–228, doi:10.1016/0273-1177(91)90460-2.

Wenzler, T., S. K. Solanki, N. A. Krivova, and D. M. Fluri (2004), Comparison between KPVT/SPM and SoHO/MDI magnetograms with an application to solar irradiance reconstructions, *Astron. Astrophys.*, *427*, 1031–1043, doi:10.1051/0004-6361:20041313.

Wenzler, T., S. K. Solanki, N. A. Krivova, and C. Fröhlich (2006), Reconstruction of solar irradiance variations in cycles 21–23 based on surface magnetic fields, *Astron. Astrophys.*, *460*, 583–595, doi:10.1051/0004-6361:20065752.

White, S. M. (1999), Radio versus EUV/X-ray observations of the solar atmosphere, *Sol. Phys.*, *190*, 309–330, doi:10.1023/A:1005253501584.

White, S. M., and M. R. Kundu (1997), Radio observations of gyroresonance emission from coronal magnetic fields, *Sol. Phys.*, *174*, 31–52.

Worden, J., and J. Harvey (2000), An evolving synoptic magnetic flux map and implications for the distribution of photospheric magnetic flux, *Sol. Phys.*, *195*, 247–268.

C. N. Arge, C. J. Henney, and S. M. White, Space Vehicles Directorate, Air Force Research Laboratory, 3550 Aberdeen Ave., SE, Kirtland AFB, NM 87117, USA. (cjhenney@gmail.com)

W. A. Toussaint, National Solar Observatory, 950 N. Cherry Ave., Tucson, AZ 85719, USA.

DISTRIBUTION LIST

DTIC/OCP
8725 John J. Kingman Rd, Suite 0944
Ft Belvoir, VA 22060-6218 1 cy

AFRL/RVIL
Kirtland AFB, NM 87117-5776 2 cys

Official Record Copy
AFRL/RVBXS/Charles N. Arge 1 cy